HHS Public Access

Author manuscript

Cancer Immunol Res. Author manuscript; available in PMC 2018 August 01.

Published in final edited form as:

Cancer Immunol Res. 2017 August ; 5(8): 666–675. doi:10.1158/2326-6066.CIR-17-0081.

Modulation of Endoplasmic Reticulum Stress Controls CD4+ T Cell Activation and Anti-tumor Function

Jessica E Thaxton[1,2,4], **Caroline Wallace**[1], **Brian Riesenberg**[1], **Yongliang Zhang**[1], **Chrystal Paulos**[1,2], **Craig Beeson**[3], **Bei Liu**[1,2], and **Zihai Li**[1,2]

[1]Department of Microbiology and Immunology, Medical University of South Carolina, Charleston, SC

[2]Hollings Cancer Center, Medical University of South Carolina, Charleston, SC

[3]Department of Pharmaceutical and Biomedical Sciences, Medical University of South Carolina, Charleston, SC

[4]Department of Orthopaedic Surgery, Medical University of South Carolina, Charleston, SC

Abstract

The endoplasmic reticulum (ER) is an energy-sensing organelle with intimate ties to programming cell activation and metabolic fate. T-cell receptor (TCR) activation represents a form of acute cell stress and induces mobilization of ER Ca^{2+} stores. The role of the ER in programming T-cell activation and metabolic fate remains largely undefined. Gp96 is an ER protein with functions as a molecular chaperone and Ca^{2+} buffering protein. We hypothesized that the ER stress response may be important for $CD4^+$ T-cell activation and that gp96 may be integral to this process. To test our hypothesis we utilized genetic deletion of gp96 gene *Hsp90b1* in a $CD4^+$ T cell–specific manner. We show that gp96-deficient $CD4^+$ T cells cannot undergo activation-induced glycolysis due to defective Ca^{2+} mobilization upon TCR engagement. We found that activating naïve $CD4^+$ T cells while inhibiting ER Ca^{2+} exchange, through pharmacological blockade of the ER Ca^{2+} channel inositol trisphosphate receptor (IP_3R), led to a reduction in cytosolic Ca^{2+} content and generated a pool of $CD62L^{high}/CD44^{low}$ $CD4^+$ T cells compared to wild-type (WT) matched controls. *In vivo* IP_3R-inhibited $CD4^+$ T cells exhibited elevated tumor control above WT T cells. Together these data show that ER-modulated cytosolic Ca^{2+} plays a role in defining $CD4^+$ T-cell phenotype and function. Factors associated with the ER stress response are suitable targets for T-cell based immunotherapies.

Correspondence: Dr. Zihai Li, Department of Microbiology and Immunology, Medical University of South Carolina, 86 Jonathan Lucas Street, Charleston, SC, 29425, zihai@musc.edu, Phone: 843.792.5342, Fax: 843.792.9588.

Conflicts of Interest Statement: The authors declare no potential conflicts of interest.

Author contributions

J.E.T designed and performed all experiments and prepared manuscript. C.W. and B.R. aided in experimental procedures and discussion of data. Y.Z. and B.L. provided guidance in gp96 knockout mouse genetics and husbandry strategies. C.M.P. and C.C.B. provided guidance for adoptive cellular therapy methods and metabolic assay development, respectively. Z.L. provided mentorship in experimental design, data analysis, and interpretation.

Keywords

T cell; Calcium; ER Stress; Metabolism; Adoptive Cellular Therapy

INTRODUCTION

Upon antigen recognition in the proper immunogenic context, T cells undergo multiple rounds of proliferation (1). To fulfill the bioenergetic demands of activation and expansion naive T cells undergo a metabolic shift from oxidative phosphorylation (OXPHOS) toward aerobic glycolysis (2). During the activation process, driven by T-cell receptor (TCR) engagement, a rapid rise in cytosolic Ca^{2+} occurs that intimately controls subsequent programming of T-cell differentiation and effector function (3) (4) (5). The endoplasmic reticulum (ER) maintains cell Ca^{2+} stores, and release of Ca^{2+} into the cytosol promotes T-cell activation (6) (7) (8) . In activated T cells, metabolites from the glycolytic pathway work to inhibit Ca^{2+} re-uptake by the ER to potentiate the effector T-cell metabolic cycle (9). The role of initial Ca^{2+} rise and the channels that drive this process has not been well studied in the context of the T-cell metabolic programs.

The ER houses molecular chaperones with numerous functions in the cell stress response, protein folding, and Ca^{2+} control (10) (11,12) (13). In the face of acute perturbations in cellular homeostasis, characterized by an imbalance in cellular Ca^{2+}, ER stress chaperones are mobilized at the gene and protein levels in order to restore protein homeostasis via increased protein folding and chaperoning (14). Gp96 (glucose-regulated protein, grp94) is a major ER stress protein that is a molecular chaperone and Ca^{2+} buffering protein and is responsive to changes in glucose availability (12) (15). The specific role of gp96 in metabolism and activation and the general involvement of ER stress in response to TCR engagement are unknown.

We show that acute ER stress was tied to activation, which resulted in upregulation of gp96. $CD4^+$ T cells required gp96 for activation and induction of glycolysis, in association with modulation of Ca^{2+} mobilization. We elucidated a role for Ca^{2+} in programming $CD4^+$ activation and differentiation and demonstrated that the ER-Ca^{2+} axis can be targeted to modulate $CD4^+$ T-cell phenotype and metabolic dependence. Direct inhibition of the inositol triphosphate receptor (IP_3R), the ER-mitochondrial Ca^{2+} channel, resulted in a pool of $62L^{high}/CD44^{low}$ $CD4^+$ T cells with increased spare respiratory capacity compared to untreated control T cells that produced better antitumor activity *in vivo*.

MATERIALS & METHODS

Mice

T cell–specific deletion of gp96 on a C57BL/6J background was accomplished by crossing *Hsp90b1*$^{flox/flox\ (16)}$ mice with *Cd4-Cre* (Tg(Cd4-cre)1Cwi/BfluJ) transgenic mice (The Jackson Laboratory). C57BL/6J, *Rag1*$^{-/-}$ (B6.129S7-*Rag1*^{tm1Mom}/J), OT-1 (C57BL/6-Tg(TcraTcrb)1100Mjb/J), TRP-1 (B6.Cg-*Rag1*^{tm1Mom} *Tyrp1*$^{B\text{-}w}$ Tg(Tcra,Tcrb)9Rest/J), or BALB/cJ mice were purchased from Jackson Laboratories. Ly5.2 (B6.SJL-*Ptprc*^{a} *Pepc*^{b}/

BoyJ) mice were a kind gift of Dr. Xue-Zhong Yu. All animal experiments were approved Medical University of South Carolina (MUSC) Institutional Animal Care and Use Committee and the Division of Laboratory Animal Resources at MUSC maintained all mice.

Human Samples

This work was determined by MUSC Institutional Review Board to be exempt under protocol PRO55960. Normal donor patients undergoing routine non-cancer associated surgery were consented under MUSC Biorepository surgical consent forms and samples were de-identified. Studies were conducted in accordance with the Declaration of Helsinki, International Ethical Guidelines for Biomedical Research Involving Human Subjects (CIOMS), Belmont Report, or U.S. Common Rule. Blood (5mL) was collected in EDTA coated tubes and PBMC were isolated via Histopaque centrifugation (Sigma).

RT-PCR and Immunoblot Analysis

RNA was isolated with RNeasy Mini Kit (QIAGEN) and single-strand cDNA was made with High Capacity RNA-to-cDNA Kit (Applied Biosystems, Thermo Fisher). Taqman gene expression assays (Applied Biosystems, Thermo Fisher) were used to perform real-time PCR using the StepOnePlus Real-Time PCR system (Applied Biosystems, Thermo Fisher). mRNA expression for *grp94* and *grp78* was normalized to *GAPDH*. For immunoblot cell lysates of naïve $CD4^+$ T cells bead sorted from thymus or spleen (Miltenyi) were prepared. Lysates were probed with gp96 antibody (Enzo Life Sciences) or β-actin control (Sigma).

Flow Cytometry

The following fluorochrome-conjugated monoclonal antibodies were purchased from BD Pharmingen (FITC-vβ14 (14-2), FITC-BrDU (Bu20)) and eBioscience (FITC or APC-CD4 (GK1.5), APC-CD8 (53-6.7), FITC, PE, or Percp-Cy5.5-CD62L (MEL-14), PE-CD18 (M18/2), PE-Cy7-CD44 (IM7), APC-Cy7-CD45.1 (A20), V450-CD45.2 (ID4), PE-CD45RO (UCHLI), PE-Cy7-CD62L (DREG-56), APC-CD4 (OKT4). PE-Gp96 (9G10) intracellular monoclonal antibody and respective isotype control were purchased from AbCAM. Extracellular stains were performed in PBS supplemented with 2% FBS. All intracellular stains, unless otherwise noted below, were performed with Foxp3/Transcription Factor intracellular staining buffer (eBioscience). For BrDU stain BrDU FACS kit and protocol were used (BD Bioscience). Cytosolic Ca^{2+} (Fluo-4, 0.5 μM), mitochondrial Ca^{2+} (Rhod-2, 2 μM), and mitochondrial membrane potential (TMRM, 10 nM) dyes (Molecular Probes) were loaded at 37°C for 30 minutes in warm PBS and extracellular stains were added post dye incubation. Samples were run directly on flow cytometer.

In vitro plate-bound and peptide activation

For primary T cell activations of WT or 96KO splenocytes, $CD4^+$ or $CD8^+$ T cells were isolated with naïve $CD4^+$ T cell or $CD8^+$ T cell isolation kits (Miltenyi) and cultured for 18 h with plate-bound aCD3 and soluble CD28 (ebioscience) with IL2 (NCI). Splenocytes from TRP-1 TCR transgenic mice were cultured with cognate peptide-loaded irradiated (10Gy) WT splenic feeder cells and plated. Total splenocytes from OT-1 TCR transgenic mice were pre-incubated with OVA peptide and plated.

Microscopy

Naïve bead-isolated $CD4^+$ T cells (Miltenyi) were counted and loaded with Fluo-4 (0.5 μM, Molecular Probes) in T cell media for 30 min at 37°C. Cells were labeled with CD4-APC and spun onto poly-lysine coated plates (Tissue-Tec) and fresh media was added. Imaging was performed using the Olympus FV10 for 148 frames at 11s intervals directly after addition of CD3/28 beads (DynaBeads). Fiji Image J software was used to quantify Fluo-4 fluorescence over time on a single cell basis.

Metabolic Assays

Oxygen consumption rates (OCR) and extracellular acidification rates (ECAR) were measured in non-buffered RS media supplemented with HEPES under basal conditions and in response to 1μM oligomycin, 1.5 μM FCCP, and 100 nM rotenone + 1 μM Antimycin A (OCR) or 10 μM glucose, 1 μM oligomycin, and 10 μM 2-deoxyglucose (ECAR) with XF-96 Extracellular Flux Analyzer (Seahorse Bioscience). Cell Taq was used for T cell adherence. For *in vivo* 2-NBDG (Cayman Chemical) uptake, 100 μg/mouse was injected via tail vein and mice were bled 15 minutes post injection. *Ex vivo* 2-NBDG uptake was assessed 18 h post T-cell activation after glucose-free medium treatment. Lactate in cell culture media was measured with Lactic Acid kit (Sigma).

Adoptive Cellular Therapy (ACT)

B16F10 cells were obtained from ATCC and tested negative for mycoplasma in March 2015. Cells were passaged three times prior to *in vivo* inoculation. All media used was supplemented with plasmocin prophylactic (Invivogen). Cells were not re-authenticated during the course of these experiments. Tumors were established on the right flank of C57BL/6 male mice for 7 days. One day prior to ACT mice were irradiated (5Gy). *Ex vivo*–expanded TRP-1 TCR-transgenic T cells (2×10^6) treated for 7 days with vehicle or 2-APB were injected into the tail vein and tumor growth was assessed every other day until the endpoint tumor size ($\geq 400mm^2$) was reached. For tumor-infiltrating lymphocyte (TIL) analysis, a tumor dissociation kit (Miltenyi) was used.

RESULTS

The ER stress chaperone gp96 is upregulated in response to TCR activation

Due to the fact that ER stress chaperone gp96 folds proteins, such as the integrins, which are involved in various T-cell functions, we asked whether the chaperone itself was modulated in response to T-cell activation (12) (13) (17). We purified $CD4^+$ or $CD8^+$ T cells from wild-type (WT) mouse spleens and assessed gp96 gene expression after 6 and 18 h of activation. Both $CD4^+$ and $CD8^+$ T cells upregulated gp96 gene expression 6 and 18 h post activation, indicating acute ER stress response (Fig. 1A and B). To determine whether TCR activation induces the generalized ER stress response-associated with increased gene expression of chaperone proteins, we measured grp78 expression in the aforementioned conditions in both $CD4^+$ and $CD8^+$ T cells. In line with a general and acute ER stress response, grp78 gene expression was also increased at 6 h and 18 h post T-cell activation (Supplementary Fig. S1). To confirm the gene product of gp96 we measured gp96 protein expression via intracellular

staining and flow cytometry at 18 h post T-cell activation in both $CD4^+$ and $CD8^+$ T cells. At this time point gp96, as measured by mean fluorescent intensity (MFI), was significantly upregulated in both $CD4^+$ and $CD8^+$ T-cell subsets well above unstimulated naïve controls (Fig. 1C).

Due to the upregulation of gp96 gene and protein in both $CD4^+$ and $CD8^+$ T cells upon CD3/28 activation (Fig. 1A–C), we asked whether this response was specific to TCR activation induced by cognate MHC class I–peptide complexes. We assessed the $CD4^+$ T cell response using T cells from TCR transgenic mice with a TCR specific for tyrosinase-related protein-1 (TRP-1). $CD4^+$ T cells were activated for 18 h in the presence of cognate peptide, and the induction of intracellular gp96 was measured. TCR transgenic $CD4^+$ T cells had significantly increased gp96 protein expression in response to cognate peptide, compared to naïve $CD4^+$ T-cell controls (Fig. 1D) (18). We next measured induction of gp96 in OT-1 TCR transgenic $CD8^+$ T cells specific for chicken ovalbumin peptide, (19). Similar to $CD4^+$ T cells, activation of $CD8^+$ T cells with cognate antigen induced gp96 protein expression (Fig. 1E). Given the critical role of the acute ER stress response in cellular activation and differentiation, our results agree with published data (20). However, our data demonstrate that TCR ligation is a form of acute stress that can induce ER stress chaperones in both primary $CD4^+$ and $CD8^+$ T cells.

T cell-specific gp96 mutants have altered $CD4^+$ T-cell subsets

We have previously demonstrated that the function of regulatory T cells is greatly impaired by deletion of gp96, due to loss of GARP, which is a client protein of gp96 (17). We now investigated whether gp96 deficiency in the effector cell subset may impact T-cell activation and phenotype. We generated $CD4^+$ T cell–specific gene deletion mutants for gp96 via CD4*cre* × *Hsp90b1*$^{flox/flox}$ (96KO) genetic cross and confirmed gene deletion and loss of protein expression in naïve $CD4^+$ bead–isolated fractions from both spleen and thymus (Supplementary Fig. S2A and B). Given reduced gp96 protein expression in CD4 single-positive (SP) thymocytes, we measured the expression of thymic differentiation markers CD25, CD44, and CD127 among WT or 96KO mice and found no differences (data not shown). To assess alterations in SP and double-positive (DP) thymocyte subsets we measured $CD4^+$/$CD8^+$ T cells among thymocytes and found no differences in the size of the DP populations between WT or 96KO groups (Fig. 2A–C). Given that we aimed to assess the role of gp96 in T-cell activation, we examined TCR Vβ chain usage via flow cytometry in WT and 96KO mice. In both spleen and thymus, 14 commonly expressed Vβ chains were expressed to a similar extent in both WT and 96KO mice (Supplementary Fig. S2C).

CD4*cre*, expressed in the double-positive stage of thymoctye maturation, induced loxp-mediated gp96 gene deletion in >90% of $CD4^+$ and $CD8^+$ T cells. We undertook phenotypic analysis of $CD4^+$ and $CD8^+$ thymocytes, splenocytes, and lymph node-associated populations between WT and 96KO mice (21). In agreement with our protein and gene deletion data (Supplementary Fig. S2A and B) we found that splenic populations were significantly reduced in gp96 expression in both $CD4^+$ and $CD8^+$ T-cell subsets (Fig. 2A). We noticed that splenic populations of $CD4^+$ T cells significantly increased in 96KO mice compared to WT controls. $CD8^+$ T-cell percentages in 96KO mice appeared slightly reduced

(Fig. 2B and C, Supplementary Table S1). Our lab has shown that gp96 chaperones multiple integrins, many of which are essential for T-cell homing to lymph nodes. Thus, a direct functional consequence of T cell–specific gene deletion of gp96, was reduced percentages of $CD4^+$ and $CD8^+$ T cells that had trafficked to mesenteric lymph nodes in 96KO mice compared to WT controls (Fig. 2B and C, Supplementary Table S1) (13).

Analysis of absolute T-cell numbers in both $CD4^+$ and $CD8^+$ T-cell subsets showed that absolute $CD8^+$ T-cell numbers between WT and 96KO mice were not significantly different. However, the absolute numbers of $CD4^+$ T-cell populations were affected at absolute levels between WT and 96KO mice (Supplementary Fig. S3A, Supplementary Table S1). Assessment of subpopulations of $CD4^+$ T cells in spleens showed an increase in percent $CD44^+/CD4^+$ T cells indicative of activated and differentiated T cells in 96KO mice compared to WT controls (Fig. 2D and E). Detailed analysis of subpopulations via absolute quantification unveiled that all subpopulations within 96KO splenocytes were significantly elevated (Fig. 2F).

Loss of gp96 results in $CD4^+$ T-cell activation defects

In order to rectify the finding that although 96KO mice possessed greater numbers of both naive and less activated $CD4^+$ T cell, they also had highly activated $CD44^+$ T cells, we used the gp96-folded molecule CD18 as a marker of gp96 deletion *in vivo* among $CD4^+$ T-cell subsets. Our data show that the highly activated $CD44^+$ T-cell subset in 96KO mice was an outgrowth of a remnant WT population (Supplementary Fig. 3B). To further substantiate this finding and investigate the role of gp96 in $CD4^+$ T-cell activation, we CFSE-labeled $CD4^+$ T cells isolated from splenocytes of WT or 96KO mice (depleted of $CD4^+/CD25^+$ cells), and transferred them into sublethally irradiated $RAG1^{-/-}$ mice. Aftter 14 days we assessed splenic populations of recipient $RAG1^{-/-}$ mice for $CFSE/CD62L^+$ populations. Transfers from 96KO mice contained $CFSE^+/CD62L^+$ populations, whereas transfers from WT mice showed complete activation, as shown by robust cell division and loss of $CFSE^+$ transferred $CD4^+$ T cells (Supplementary Fig. S4). due to loss of Treg function (17). To address the role of a cell intrinsic activation defect in 96KO $CD4^+$ T cells not due to loss of Treg function, we undertook mixed bone marrow chimera analysis. As Fig. 3A indicates, T cell-depleted bone marrow

Ca^{2+} flow and mitochondrial membrane potential in $CD4^+$ 96KO T cells

ER stress response is tightly tied to fluctuations in cell Ca^{2+} concentrations. ER-associated and chaperone proteins have secondary capacities as Ca^{2+} buffering proteins (15,23). For example, T cell–specific deletion of calreticulin greatly impairs cell Ca^{2+} oscillations resultant in a pool of less activated T cells and autoimmune conditions *in vivo* (24). We undertook *ex vivo* Ca^{2+} imaging of single cells from WT or 96KO naïve $CD4^+$ T-cell preparations. Bead-isolated naïve WT or 96KO $CD4^+$ T cells were labeled with cytosolic Ca^{2+} imaging dye Fluo-4. This dye fluoresces upon cytosolic free Ca^{2+} elevation. We pre-labeled $CD4^+$ T cells with Fluo-4 and live-imaged fluorescent signal upon CD3/28 bead addition. Fluorescence in WT $CD4^+$ T cells increased over the first 30 minutes of TCR engagement, whereas 96KO $CD4^+$ T cells did not mobilize cytosolic free Ca^{2+} similar to WT patterns (Fig. 4A). Direct quantification of mobilization was obtained by measurement

of peak Ca^{2+} intensity with the first 30 minutes of TCR ligation between WT and 96KO groups (Fig. 4B). 96KO $CD4^+$ T cells did not mobilize cytosolic free Ca^{2+} to the extent that WT $CD4^+$ T cells did, lending potential mechanistic support to explain the activation defect in 96KO $CD4^+$ T cells. However, more work is needed to attribute this effect directly to the Ca^{2+} buffering capacity, and not the chaperone function, of gp96.

Given that 96KO $CD4^+$ T cells maintained a naïve state *in vivo* and that these cells showed impaired initial Ca^{2+} mobilization in response to TCR activation (Fig. 3 & Fig. 4A), we asked whether activation-induced long-term cytosolic Ca^{2+} concentrations were impaired in these cells. We found that though naïve cytosolic Ca^{2+} concentrations between WT and 96KO cells did not differ, 18 h post-activation 96KO $CD4^+$ T cells showed significantly diminished cytosolic free Ca^{2+} (Fig. 4C). Thus, naive $CD4^+$ T cells maintained low cytosolic Ca^{2+} concentrations, which supported the notion of Ca^{2+} as a driver of T-cell activation.

Release of ER Ca^{2+} stores leads to elevated mitochondrial Ca^{2+} modulated through the IP_3R (25). Though not yet described in T cells, mitochondrial activation through cell Ca^{2+} is a key regulator of cell bioenergetics (26) (27). We asked whether inhibition of mitochondrial Ca^{2+} signal could be detected in activated 96KO $CD4^+$ T cells. We used Rhodamine-2 (Rhod-2) to assess mitochondrial Ca^{2+} content 0 and 18 h post T-cell activation. We found that, although no basal differences in mitochondrial Ca^{2+} could be detected, activated 96KO cells showed impaired mitochondrial Ca^{2+} content compared to WT T cells (Fig. 4D). These data suggested a link between ER-modulated Ca^{2+} signals and mitochondrial activation. Ca^{2+} overload within the mitochondria can lead to induction of apoptotic signaling cascade, whereas impaired mitochondrial Ca^{2+} uptake can compromise mitochondrial metabolism (28). We used the mitochondrial membrane potential dye tetramethylrhodamine methyl ester (TMRM) to measure mitochondrial activity. We reasoned that initial loss of Ca^{2+} uptake in 96KO cells would lead to inactive mitochondria as assessed by TMRM and demonstrate that mitochondrial metabolism was compromised in these cells. Indeed, 18 h after activation, WT cells increased TMRM fluorescence compared to 0 hour controls, but 96KO cells were unable to significantly regulate TMRM levels to that of WT controls (Fig. 4E). Together these data present evidence for the role of cell Ca^{2+} to modulate mitochondrial metabolism in T cells.

Gp96 $CD4^+$ T-cell mutants are impaired in glucose consumption

The role of ER stress chaperones and sensors in T-cell biology and associated metabolomics has not been studied. Upon $CD4^+$ T-cell activation, glucose uptake and entry into glycolysis is modulated by Glut-1 cell surface expression (29). Further, it is known that cytosolic Ca^{2+} can perpetuate glycolysis as glycolytic product phosphoenolpyruvate (PEP) directly inhibits ER-re-establishment of Ca^{2+} homeostasis (9). However, the role of initial mobilization of Ca^{2+} in promotion of glycolysis has not been addressed. We utilized 96KO $CD4^+$ T cells as a tool to study the induction of glycolysis within the first 18 h of T-cell activation in the context of impaired Ca^{2+} mobilization.

We asked whether there were *in vivo* differences between WT $CD4^+$ and 96KO $CD4^+$ T cells in ability to consume glucose. We injected fluorescent glucose analog 2-[N-(7-nitrobenz-2-oxa-1,3-diaxol-4-yl)amino]-2-deoxyglucose (2-NBDG) into WT or 96KO mice

and measured *in vivo* glucose uptake in $CD4^+$ populations in peripheral blood (30). 96KO $CD4^+$ T cells were severely impaired in their ability to uptake glucose compared to WT matched controls (Fig. 5A). These results were not unexpected given that cytosolic Ca^{2+} concentrations may be slightly affected *in vivo* in the context of homeostatic proliferation in 96KO T cells and highlight the importance of basal glucose uptake impacted by gp96 *in vivo* for cell survival.

In the context of 18 hour TCR activation we saw impaired glucose uptake measured by *in vitro* 2-NBDG in $CD4^+$ T cells (Fig. 5B). In accordance with diminished processing of glucose, we found that end-stage glycolytic product lactate was significantly reduced in 96KO $CD4^+$ T cells (Fig. 5C). 96KO cells activated for 18 h were also unresponsive to glucose addition, as measured by extracellular acidification rate (ECAR) in comparison to WT control rates (Fig. 5D). Thus, both gp96 and Ca^{2+} mobilization may be required for $CD4^+$ T-cell activation and subsequent induction of glycolysis.

Cytosolic Ca^{2+} defines $CD4^+$ T-cell activation and differentiation

Naïve $CD8^+$ T cells activated in the presence of glycolysis inhibitor 2-deoxyglucose (2-DG) primarily form T memory cells *in vitro* as marked by preferential dependence on oxidative metabolism (31). Given the emerging role of metabolomics in programming T-cell lineages coupled to our finding that Ca^{2+} inhibited $CD4^+$ T cells showed severe defects in glucose uptake, we asked whether cytosolic Ca^{2+} alone could define murine $CD4^+$ T-cell activation and differentiation. We harvested splenocytes from WT mice and used Fluo-4 dye to assess cytosolic free Ca^{2+} content in $CD4^+$ T cells directly *ex vivo*. Cytosolic Ca^{2+} concentrations could definitively differentiate naïve ($CD62L^+/CD44^-$), central memory ($CD62L^+/CD44^+$), and effector ($CD62L^-/CD44^+$) subsets among $CD4^+$ T-cell populations in mice (Fig. 6A–B). *In vivo* analysis of $CD8^+$ splenocytes from mice showed that cytoplasmic Ca^{2+} content was only able to differentiate $CD44^+$ effector subsets from naïve and central memory groups (Supplementary Fig. S5A). However, in the context of *in vitro* cytokine driven differentiation of $CD8^+$ T cells toward effector (IL2) or memory (IL15) lineages cytosolic Ca^{2+} was able to discriminate subsets (Supplementary Fig. S5B). Thus, cytosolic Ca^{2+} is a means to discriminate T-cell lineages and suggest that mechanisms of Ca^{2+} control may be used to modulate lineage outcomes.

We next asked whether a similar differentiation based on cytosolic free Ca^{2+} content could be made among human $CD4^+$ populations. We isolated peripheral blood mononuclear cells (PBMC) from donors and utilized CD62L/CD45RO subset analysis to differentiate between naïve ($CD62L^+/CD45RO^-$), central memory ($CD62L^+/CD45RO^+$), effector memory ($CD62L^-/CD45RO^+$), and effector ($CD62L^-/CD45RO^-$) subsets. Indeed, we found that in human $CD4^+$ T cells, cytosolic Ca^{2+} content could distinguish $CD4^+$ lineage populations. Among four PBMC samples assessed there were no significant differences between naïve and central memory cytosolic Ca^{2+} levels, whereas Ca^{2+} was able to distinguish both effector memory and effector populations from the naïve group (Supplementary Fig. S6).

Our demonstration that a low cytosolic free Ca^{2+} signal is a property able to differentiate fully activated effector T-cell populations, coupled to our finding that inhibition of Ca^{2+} mobilization impairs glucose dependence, led us to ask whether direct inhibition of ER-

mitochondrial Ca^{2+} exchange could modulate $CD4^+$ T-cell phenotype and metabolic dependence. The IP_3R is responsible for release of ER Ca^{2+} stores to both the cytosol and mitochondria, and similar to 96KO $CD4^+$ T-cell phenotype, T cell–specific deletion of IP_3R inhibits T-cell activation (25) (32). However, the specific role of IP_3R inhibition in the context of $CD4^+$ T-cell activation has not been addressed. We used IP_3R inhibitor 2-aminoethoxydiphenyl borate (2-APB) to inhibit IP_3R at the time of T-cell activation in $CD4^+$ TCR transgenic T cells. As expected, 18 h after peptide-specific activation of TRP TCR transgenic $CD4^+$ T cells, cytosolic Ca^{2+} was significantly diminished in the IP_3R inhibited T-cell group (Fig. 6C). After 7 days, TCR transgenic T cells activated in the presence of 2-APB maintained a significantly increased $CD62L^{high}$ T-cell pool with less fully activated $CD44^+$ T cells, compared to WT matched controls (Fig. 6D). Measurements for CD62L and CD44 MFI between WT or IP_3R-inhibited (IP_3RI) populations showed significantly increased CD62L expression and reduced CD44 expression in IP_3RI $CD4^+$ T cells compared to WT controls (Fig. 6E–F).

A hallmark feature of $CD62L^{high}/CD44^+$ $CD8^+$ T cells is elevated spare respiratory capacity (SRC) demonstrative of continued oxygen consumption in the context of activation (33). Given the striking $CD62L^{high}/CD44^{low}$ phenotype of IP_3RI derived $CD4^+$ T cells, we measured oxygen consumption rates (OCR) and associated SRC in these cells 7 days after initial activation. We found IP_3RI $CD4^+$ T cells possessed greater OCR and marked SRC compared to WT matched controls (Fig. 6G).

Modulation of cell Ca^{2+} enhances therapeutic efficacy of tumor-specific T Cells

A hallmark feature of T cells shifted toward a $CD62L^{high}/CD44^+$ phenotype through metabolomic modulation is elevated tumor control above glycolytic effector counterparts. Such manipulations are well documented in $CD8^+$ T-cell populations and not yet flourished among $CD4^+$ T-cell counterparts (31) (34). We asked whether IP_3RI $CD4^+$ T cells possessed the *in vivo* property of augmented tumor control. We adoptively transferred $CD4^+$ TCR transgenic T cells activated and expanded in the presence of vehicle or 2-APB into syngeneic B16F10 melanoma-bearing mice. We found that IP_3RI 2-APB–treated T cells significantly inhibited tumor growth and extended survival times above vehicle matched control T cells (Fig. 7A–B).

Possible reasons for superior tumor control by $CD62L^{high}/CD44^+$ populations are increased lymph node homing and tumor entry due to expression of CD62L and energy reserves endowed by heightened SRC (35) (33). Given that IP_3RI TRP $CD4^+$ T cells showed increased CD62L expression and elevated SRC compared to effector matched controls, we asked whether more $V\beta14^+$ CD4 T cells were found in IP_3RI T cell treated mice. Spleens from mice adoptively transferred with IP_3RI T cells showed significantly increased $V\beta14^+$ percentages and absolute numbers compared to WT matched controls (Fig. 7C and E). Phenotypic analysis of the Vβ14 populations found in mice treated with control or treated or IP_3RI-treated T cells showed that IP_3RI populations maintained significantly increased numbers of $CD62L^{high}/CD44^+$ associated populations compared to vehicle treated T-cell group (Fig. 7D). As expected, IP_3RI T cell–treated mice had significantly increased total $CD4^+$ T-cell numbers accumulated in tumors as compared to vehicle treated T-cell controls

(Fig. 7E). Together, these data show that cytosolic Ca^{2+} content was a novel property of antitumor immunity that could predict efficacy of adoptively transferred T cells.

DISCUSSION

This work depicts the initial exploration of a vivid role for the ER in T-cell biology in both control of mitochondrial function and lineage fate. The defects in 96KO $CD4^+$ T cells were not unexpected due to the essential role of this chaperone protein in general immune cell biology previously elucidated by our laboratory (36) (16). Still, the profound impairment presented in 96KO T cells is particularly intriguing given that we show that antigenic stimulation specifically upregulates the general ER stress response. Glucose-regulated proteins were discovered due to their upregulation in the context of glucose deprivation (37). In the face of acute cell stress, ER chaperones are mobilized at both the gene and protein levels to promote protein-folding functions in order to restore cellular homeostasis (38). It stands to reason that, as we have demonstrated, TCR engagement imparts a form of acute cell stress, as measured by upregulation of gp96 and grp78 gene and protein expression. Entry into glycolysis, a time of vigorous new protein synthesis, likely demands increased ER chaperone activity to support de novo protein biosynthesis.

In the context of TCR engagement, the specific role of the ER to promote T-cell metabolism has, to this point, remained largely unknown. We demonstrated that gp96 deficient $CD4^+$ T cells have defective Ca^{2+} mobilization upon TCR engagement and are unable to undergo activation-induced glycolysis. The T-cell defect in the absence of gp96 is likely multi-factorial and cannot be attributed to dysregulation of Ca^{2+} mobilization only. However, we specifically addressed the roles of ER Ca^{2+} exchange in the context of TCR engagement in $CD4^+$ T-cell activation using pharmacological inhibitors of IP_3Rs. We found that that inhibition of IP_3Rs in T cells results in a critical activation defect, followed by an inability to initiate glycolysis, consistent with the inability to mobilize cytosolic Ca^{2+} content (32). If results from other cell types may be extrapolated, IP_3R-mediated Ca^{2+} release is a key driver of mitochondrial programming and function. Deletion of IP_3Rs from B-lymphocytes show diminished mitochondrial Ca^{2+} uptake resulting in impaired cellular bioenergetics (39).

Cytosolic Ca^{2+} content was able to directly discriminate both $CD4^+$ and $CD8^+$ T-cell lineage fates. We thus reasoned that direct graded modulation of ER-mitochondrial Ca^{2+} exchange might similarly tune T-cell outcomes. Our data show that direct modulation of a second messenger ion could shift $CD4^+$ T-cell fates. This was interesting given that costimulatory signals associated with graded crosslinking of CD28 drive IP_3R-associated cytosolic Ca^{2+} rise only at the strongest levels of engagement (40).

We found *in vivo* that $CD4^+$ T cells activated in the presence of IP_3RI had augmented antitumor responses. Therapeutic efficacy of $CD4^+$ T cells in the context of adoptive cellular therapy generally involves intense cytokine conditioning (18). However, the requirements for generating therapeutically effective $CD4^+$ T cells could be tempered simply by Ca^{2+} channel modulation. Together, our data suggest a role for Ca^{2+} in programming $CD4^+$ T-cell fates, and shed light on ER-mitochondrial crosstalk in T cells that may regulate cellular bioenergetics, survival, and function *in vivo*.

Supplementary Material

Refer to Web version on PubMed Central for supplementary material.

Acknowledgments

We thank members of the Zihai Li lab and Drs. Mark Rubinstein and Matthew Scheffel for thoughtful suggestions and Gyda Beeson and Brett Hoover for Seahorse support and guidance.

Financial Support: NIH grants: CA186866, CA188419, AI070603 and AI077283 (to Z.L.), and the Hollings Cancer Center's Cancer Center K12 support and ACS (to J.E.T.).

References

1. Williams MA, Bevan MJ. Effector and memory CTL differentiation. Annual review of immunology. 2007; 25:171–92. DOI: 10.1146/annurev.immunol.25.022106.141548
2. Buck MD, O'Sullivan D, Pearce EL. T cell metabolism drives immunity. The Journal of experimental medicine. 2015; 212(9):1345–60. DOI: 10.1084/jem.20151159 [PubMed: 26261266]
3. Feske S. Calcium signalling in lymphocyte activation and disease. Nature reviews Immunology. 2007; 7(9):690–702. DOI: 10.1038/nri2152
4. Le Borgne M, Raju S. Real-Time Analysis of Calcium Signals during the Early Phase of T Cell Activation Using a Genetically Encoded Calcium Biosensor. 2016; 196(4):1471–9. DOI: 10.4049/jimmunol.1502414
5. Weber KS, Hildner K, Murphy KM, Allen PM. Trpm4 differentially regulates Th1 and Th2 function by altering calcium signaling and NFAT localization. Journal of immunology (Baltimore, Md : 1950). 2010; 185(5):2836–46. DOI: 10.4049/jimmunol.1000880
6. Feske S, Giltnane J, Dolmetsch R, Staudt LM, Rao A. Gene regulation mediated by calcium signals in T lymphocytes. Nature immunology. 2001; 2(4):316–24. DOI: 10.1038/86318 [PubMed: 11276202]
7. Nohara LL, Stanwood SR, Omilusik KD, Jefferies WA. Tweeters, Woofers and Horns: The Complex Orchestration of Calcium Currents in T Lymphocytes. Frontiers in immunology. 2015; 6:234.doi: 10.3389/fimmu.2015.00234 [PubMed: 26052328]
8. Srikanth S, Gwack Y. Orai1-NFAT signalling pathway triggered by T cell receptor stimulation. Molecules and cells. 2013; 35(3):182–94. DOI: 10.1007/s10059-013-0073-2 [PubMed: 23483280]
9. Ho PC, Bihuniak JD, Macintyre AN, Staron M, Liu X, Amezquita R, et al. Phosphoenolpyruvate Is a Metabolic Checkpoint of Anti-tumor T Cell Responses. Cell. 2015; 162(6):1217–28. DOI: 10.1016/j.cell.2015.08.012 [PubMed: 26321681]
10. Zhu G, Lee AS. Role of the unfolded protein response, GRP78 and GRP94 in organ homeostasis. Journal of cellular physiology. 2015; 230(7):1413–20. DOI: 10.1002/jcp.24923 [PubMed: 25546813]
11. Eletto D, Dersh D, Argon Y. GRP94 in ER quality control and stress responses. Seminars in cell & developmental biology. 2010; 21(5):479–85. DOI: 10.1016/j.semcdb.2010.03.004 [PubMed: 20223290]
12. Ansa-Addo EA, Thaxton J, Hong F, Wu BX, Zhang Y, Fugle CW, et al. Clients and Oncogenic Roles of Molecular Chaperone gp96/grp94. Current topics in medicinal chemistry. 2016; 16(25): 2765–78. [PubMed: 27072698]
13. Staron M, Yang Y, Liu B, Li J, Shen Y, Zúñiga-Pflücker JC, et al. gp96, an endoplasmic reticulum master chaperone for integrins and Toll-like receptors, selectively regulates early T and B lymphopoiesis. Blood. 2010; 115(12):2380–90. DOI: 10.1182/blood-2009-07-233031 [PubMed: 19965672]
14. Walter P, Ron D. The unfolded protein response: from stress pathway to homeostatic regulation. Science (New York, NY). 2011; 334(6059):1081–6. DOI: 10.1126/science.1209038
15. Prins D, Michalak M. Organellar calcium buffers. Cold Spring Harbor perspectives in biology. 2011; 3(3)doi: 10.1101/cshperspect.a004069

16. Yang Y, Liu B, Dai J, Srivastava PK, Zammit DJ, Lefrancois L, et al. Heat shock protein gp96 is a master chaperone for toll-like receptors and is important in the innate function of macrophages. Immunity. 2007; 26(2):215–26. DOI: 10.1016/j.immuni.2006.12.005 [PubMed: 17275357]
17. Zhang Y, Wu BX, Metelli A, Thaxton JE, Hong F, Rachidi S, et al. GP96 is a GARP chaperone and controls regulatory T cell functions. The Journal of clinical investigation. 2015; 125(2):859–69. DOI: 10.1172/jci79014 [PubMed: 25607841]
18. Muranski P, Boni A, Antony PA, Cassard L, Irvine KR, Kaiser A, et al. Tumor-specific Th17-polarized cells eradicate large established melanoma. Blood. 2008; 112(2):362–73. DOI: 10.1182/blood-2007-11-120998 [PubMed: 18354038]
19. Hogquist KA, Jameson SC, Heath WR, Howard JL, Bevan MJ, Carbone FR. T cell receptor antagonist peptides induce positive selection. Cell. 1994; 76(1):17–27. [PubMed: 8287475]
20. Wu J, Kaufman RJ. From acute ER stress to physiological roles of the Unfolded Protein Response. Cell death and differentiation. 2006; 13(3):374–84. DOI: 10.1038/sj.cdd.4401840 [PubMed: 16397578]
21. Lee PP, Fitzpatrick DR, Beard C, Jessup HK, Lehar S, Makar KW, et al. A critical role for Dnmt1 and DNA methylation in T cell development, function, and survival. Immunity. 2001; 15(5):763–74. [PubMed: 11728338]
22. Sharma S, Zhu J. Immunologic applications of conditional gene modification technology in the mouse. Current protocols in immunology. 2014; 105 10.34.1-13. doi: 10.1002/0471142735.im1034s105
23. Koch G, Smith M, Macer D, Webster P, Mortara R. Endoplasmic reticulum contains a common, abundant calcium-binding glycoprotein, endoplasmin. Journal of cell science. 1986; 86:217–32. [PubMed: 3308928]
24. Porcellini S, Traggiai E, Schenk U, Ferrera D, Matteoli M, Lanzavecchia A, et al. Regulation of peripheral T cell activation by calreticulin. The Journal of experimental medicine. 2006; 203(2): 461–71. DOI: 10.1084/jem.20051519 [PubMed: 16492806]
25. Hogan PG, Lewis RS, Rao A. Molecular basis of calcium signaling in lymphocytes: STIM and ORAI. Annual review of immunology. 2010; 28:491–533. DOI: 10.1146/annurev.immunol.021908.132550
26. Denton RM, Randle PJ, Martin BR. Stimulation by calcium ions of pyruvate dehydrogenase phosphate phosphatase. The Biochemical journal. 1972; 128(1):161–3. [PubMed: 4343661]
27. Denton RM. Regulation of mitochondrial dehydrogenases by calcium ions. Biochimica et biophysica acta. 2009; 1787(11):1309–16. DOI: 10.1016/j.bbabio.2009.01.005 [PubMed: 19413950]
28. Duchen MR. Mitochondria and calcium: from cell signalling to cell death. The Journal of physiology. 2000; 529(Pt 1):57–68. [PubMed: 11080251]
29. Macintyre AN, Gerriets VA, Nichols AG, Michalek RD, Rudolph MC, Deoliveira D, et al. The glucose transporter Glut1 is selectively essential for CD4 T cell activation and effector function. Cell metabolism. 2014; 20(1):61–72. DOI: 10.1016/j.cmet.2014.05.004 [PubMed: 24930970]
30. O'Sullivan D, van der Windt GJ, Huang SC, Curtis JD, Chang CH, Buck MD, et al. Memory CD8(+) T cells use cell-intrinsic lipolysis to support the metabolic programming necessary for development. Immunity. 2014; 41(1):75–88. DOI: 10.1016/j.immuni.2014.06.005 [PubMed: 25001241]
31. Sukumar M, Liu J, Ji Y, Subramanian M, Crompton JG, Yu Z, et al. Inhibiting glycolytic metabolism enhances CD8+ T cell memory and antitumor function. The Journal of clinical investigation. 2013; 123(10):4479–88. DOI: 10.1172/jci69589 [PubMed: 24091329]
32. Jayaraman T, Ondriasova E, Ondrias K, Harnick DJ, Marks AR. The inositol 1,4,5-trisphosphate receptor is essential for T-cell receptor signaling. Proceedings of the National Academy of Sciences of the United States of America. 1995; 92(13):6007–11. [PubMed: 7597070]
33. van der Windt GJ, Everts B, Chang CH, Curtis JD, Freitas TC, Amiel E, et al. Mitochondrial respiratory capacity is a critical regulator of CD8+ T cell memory development. Immunity. 2012; 36(1):68–78. DOI: 10.1016/j.immuni.2011.12.007 [PubMed: 22206904]
34. Crompton JG, Sukumar M, Roychoudhuri R, Clever D, Gros A, Eil RL, et al. Akt inhibition enhances expansion of potent tumor-specific lymphocytes with memory cell characteristics.

Cancer research. 2015; 75(2):296–305. DOI: 10.1158/0008-5472.can-14-2277 [PubMed: 25432172]

35. Nolz JC, Starbeck-Miller GR, Harty JT. Naive, effector and memory CD8 T-cell trafficking: parallels and distinctions. Immunotherapy. 2011; 3(10):1223–33. DOI: 10.2217/imt.11.100 [PubMed: 21995573]
36. Liu B, Li Z. Endoplasmic reticulum HSP90b1 (gp96, grp94) optimizes B-cell function via chaperoning integrin and TLR but not immunoglobulin. Blood. 2008; 112(4):1223–30. DOI: 10.1182/blood-2008-03-143107 [PubMed: 18509083]
37. Kozutsumi Y, Segal M, Normington K, Gething MJ, Sambrook J. The presence of malfolded proteins in the endoplasmic reticulum signals the induction of glucose-regulated proteins. Nature. 1988; 332(6163):462–4. DOI: 10.1038/332462a0 [PubMed: 3352747]
38. Lee AS. The glucose-regulated proteins: stress induction and clinical applications. Trends in biochemical sciences. 2001; 26(8):504–10. [PubMed: 11504627]
39. Cardenas C, Miller RA, Smith I, Bui T, Molgo J, Muller M, et al. Essential regulation of cell bioenergetics by constitutive InsP3 receptor Ca2+ transfer to mitochondria. Cell. 2010; 142(2): 270–83. DOI: 10.1016/j.cell.2010.06.007 [PubMed: 20655468]
40. Ledbetter JA, Imboden JB, Schieven GL, Grosmaire LS, Rabinovitch PS, Lindsten T, et al. CD28 ligation in T-cell activation: evidence for two signal transduction pathways. Blood. 1990; 75(7): 1531–9. [PubMed: 2156582]

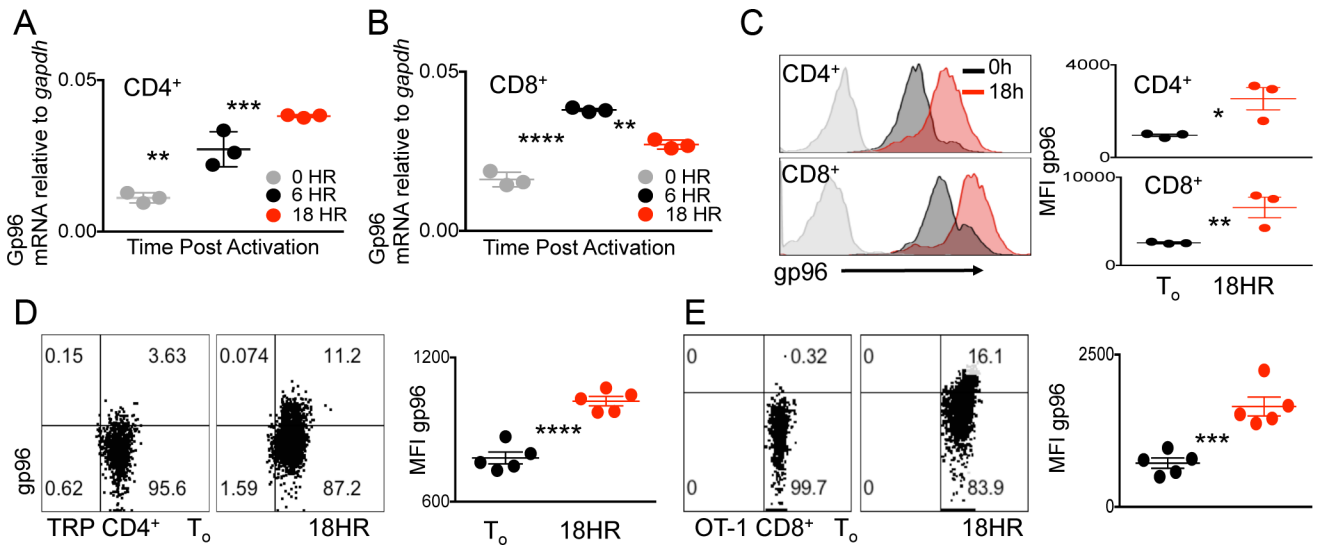

Figure 1. ER stress chaperone gp96 is upregulated in response to TCR stimulation

(A) Quantitative RT-PCR analysis of gp96 expression in naive $CD4^+$ or (B) $CD8^+$ T cells isolated from WT spleens stimulated with CD3/28 for 0, 6, or 18 hours. (C) Representative flow cytometry histogram and quantification of intracellular staining for gp96 in $CD4^+$ (top panel) or $CD8^+$ (bottom panel) T cells 0 or 18 h post CD3/28 stimulation. Isotype controls shaded in gray. Representative flow cytometry plots and quantification of intracellular gp96 levels in (D) $CD4^+$ T cells from TRP TCR transgenic mice or (E) $CD8^+$ T cells from OT-1 TCR transgenic mice at T_o or 18 h after peptide activation. Data points represent separate mice. Data are mean ± SEM. Numbers in (D) and (E) represent percentage of cell in each quadrant. $*P<0.05$, $**P<0.01$, $***P<0.001$, $****P<0.0001$, 2-tailed Student *t* test. Three independent repeats were performed for each experiment.

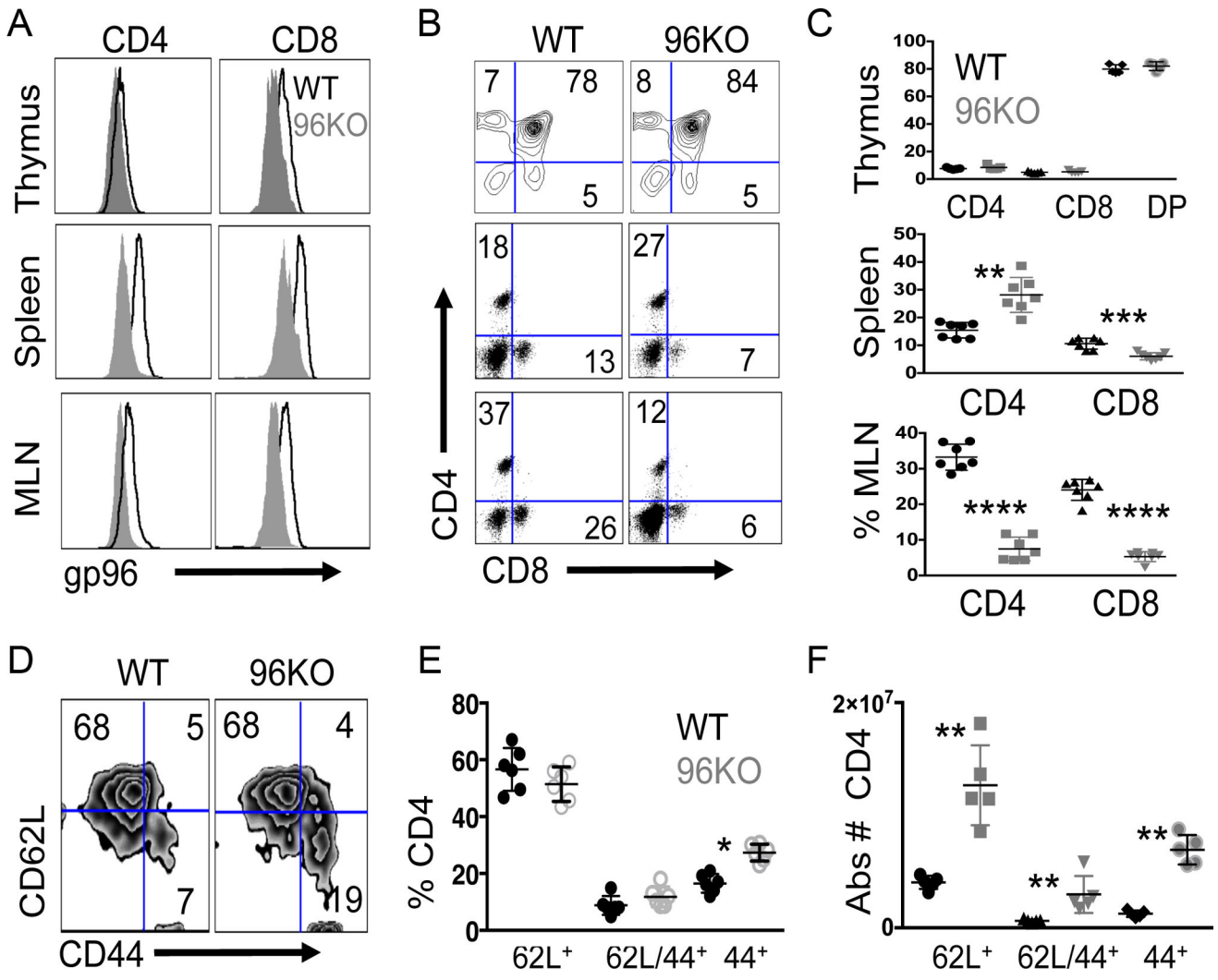

Figure 2. Gp96 T cell specific gene deletion induces CD4$^+$ subset changes

(A) Representative histograms of gp96 expression in CD4$^+$ or CD8$^+$ single-positive thymocytes, splenocytes, or mesenteric lymph node (MLN) T cells preparations from CD4*creHsp90b1*$^{flox/WT}$ (WT) or CD4*creHsp90b1*$^{flox/flox}$ (96KO) mice. (B) Representative FACS plots for CD4$^+$/8$^+$ populations from WT or 96KO mice from thymus, spleen, or MLNs and (C) quantification of populations. (D) Representative FACS plots gated from CD4$^+$/CD25$^-$ populations from WT or 96KO splenocytes and (E) percentage or (F) absolute number quantification of splenic subpopulations. Data are mean ± SD of 5–7 mice per group. *$P < 0.05$, **$P < 0.01$,****$P < 0.000,1$ 2-tailed Student *t* test.

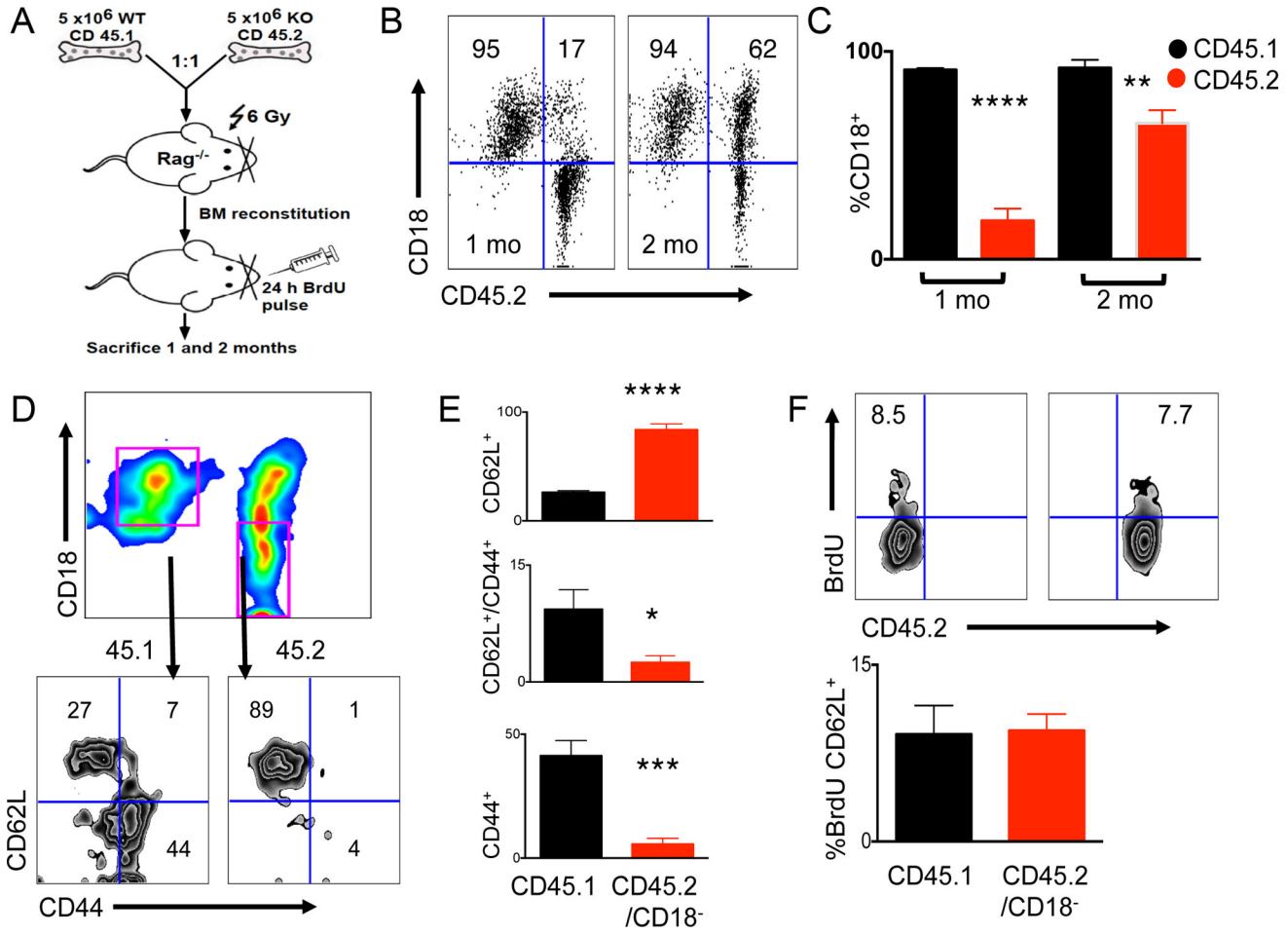

Figure 3. WT CD4$^+$ T cells outcompete 96KO CD4$^+$ T cells, indicative of a cell intrinsic defect

(A) Experimental design of 1:1 WT (CD45.1) or 96KO (CD45.2) T-cell depleted mixed bone marrow chimeras (BMC) transferred to irradiated (10Gy) *Rag1*$^{-/-}$ mice and harvested 1 and 2 months post transfer. (B) Representative flow cytometry plots of splenocytes from 1 and 2 months post bone marrow reconstitution, gated on CD4$^+$ T cells and probed for CD45.2$^+$/CD18$^-$ as a measure of gp96 deletion. (C) Quantification of CD4$^+$ T cells probed for CD45.1/CD45.2/CD18 1 and 2 months post BMC reconstitution. (D) Representative flow cytometry plots of splenocytes from 2 months post BMC reconstitution, gated on CD4$^+$ T cells and further gated from (pink gates) CD45.1/CD18$^+$ (WT) or CD45.2/CD18$^-$ (96KO) populations assessed for CD62L/CD44 expression and (E) quantification of subset populations. (F) Representative flow cytometry plots of BrdU uptake gated from CD4$^+$ splenic T cells from 24 hour pulsed 1 month BMC mice and (G) quantification of BrdU uptake in CD4/CD62L$^+$ T cells gated from WT (CD45.1/CD18$^+$) or 96KO (CD45.2/CD18$^-$) populations. Data are mean ± SD of 4 mice per group. *$P < 0.05$, **$P < 0.01$, ***$P < 0.001$, ****$P < 0.0001$, 2-tailed Student *t* test. Two independent repeats were performed for these experiments.

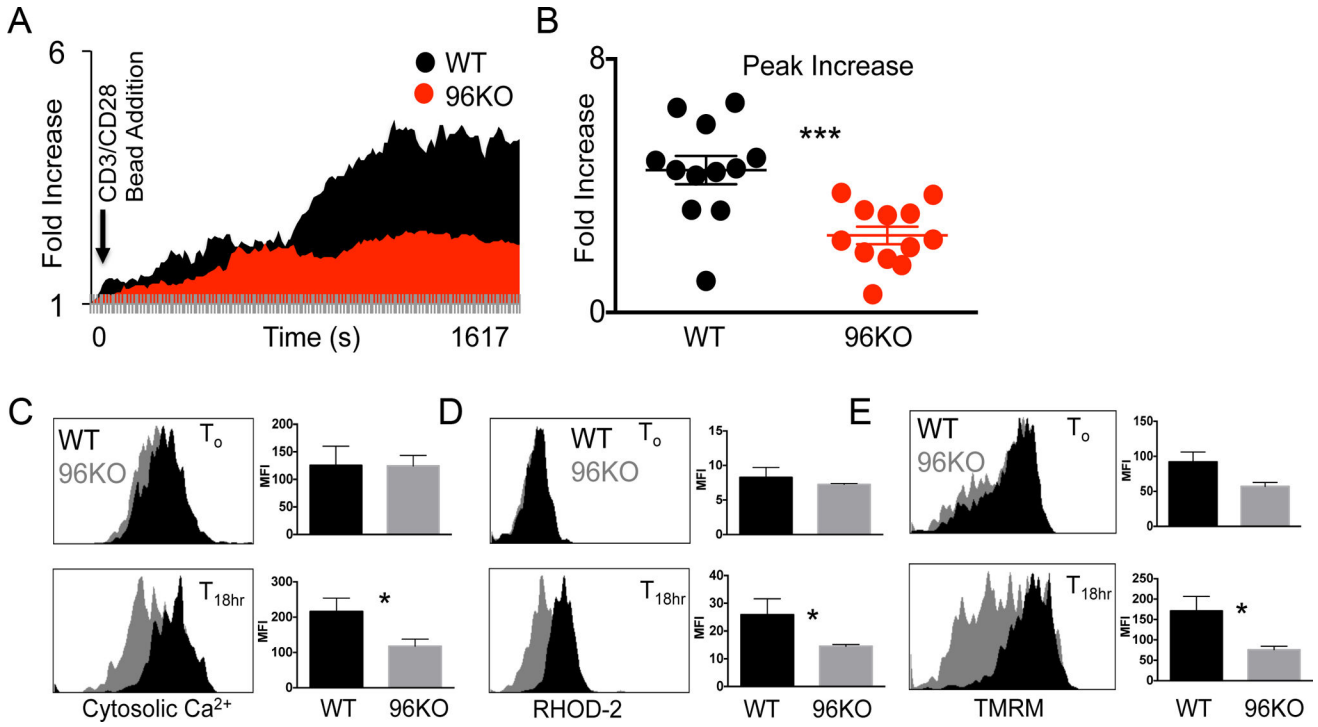

Figure 4. Gp96 is necessary for naïve CD4$^+$ T-cell mobilization of intracellular Ca^{2+}

(A) Real time single cell imaging in WT or 96KO CD4$^+$/CD62L$^+$ T cells. Naïve T cells were isolated and labeled with Fluo-2 (FITC) and CD4 (APC) and adhered to glass slide incubating chambers. At time 0 CD3/28 beads were added to media. Data are plotted as average fold increase in Fluo-4 for 12–16 cells per group over 11 second intervals for ~30 minutes. Analysis was performed with Image J software. (B) Peak fluorescent increase in Fluo-4 was recorded. Data are mean ± SEM of 12 cells per group. ***$P < 0.0001$, 2-tailed Student *t* test. Similar data were obtained for 4 mice per group in 4 separate experiments. Representative histograms and quantification from 0 or 18 hour CD3/28 activated splenocytes from WT or 96KO mice gated on CD4$^+$/CD18$^+$ (WT) or CD4$^+$/CD18$^-$ (96KO) cells and probed for (C) cytosolic Ca^{2+} with Fluo-4 (D) mitochondrial Ca^{2+} with Rhod-2 (D) or mitochondrial membrane potential with TMRM. Data are means from 3 mice, three independent experimental repeats were performed. *$P < 0.05$, 2-tailed Student *t* test.

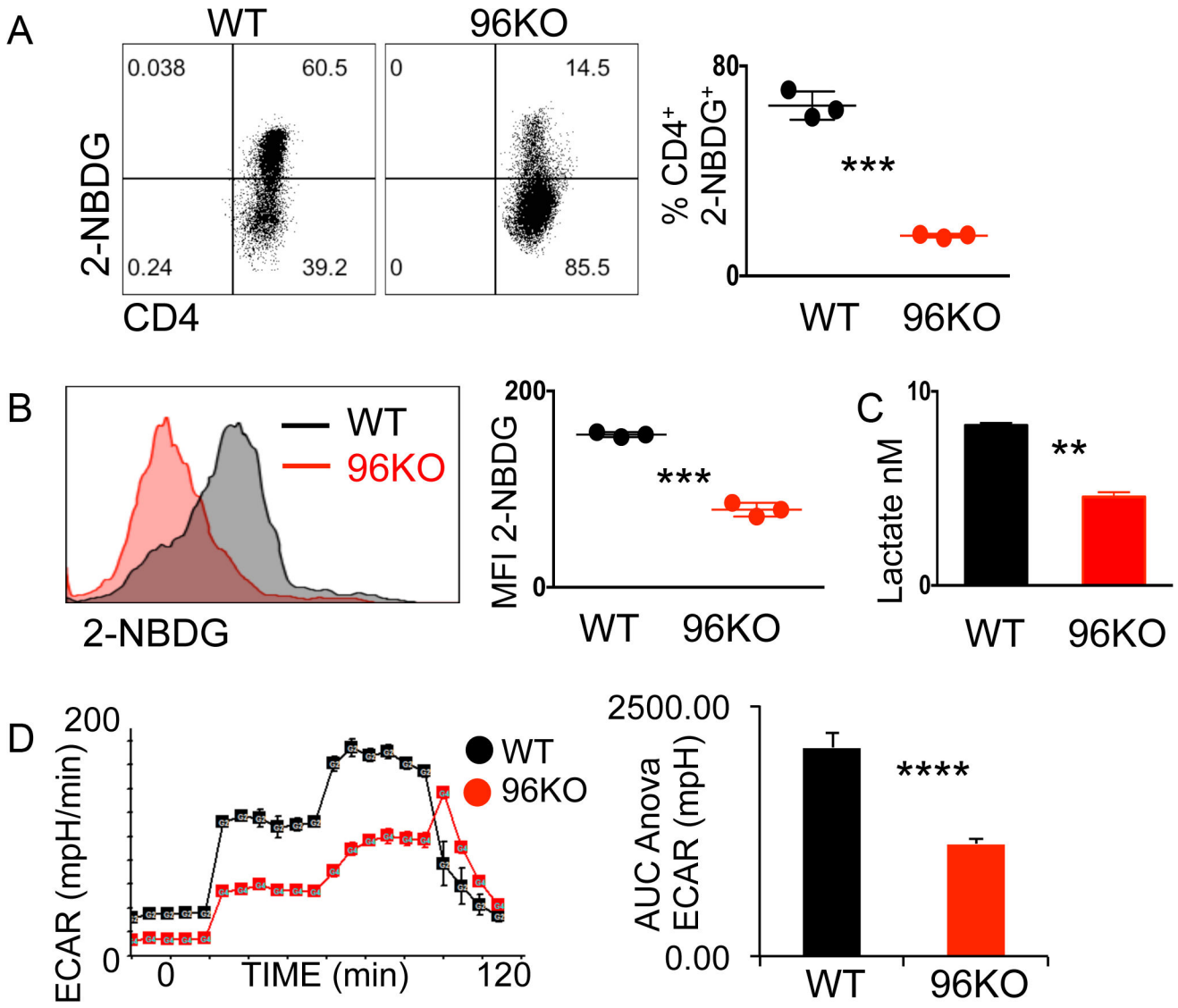

Figure 5. 96KO CD4$^+$ T cells show impaired glucose uptake

(A) Representative flow cytometry plots or (B) histograms and quantification of 2-NBDG *in vivo* and *in vitro* uptake, respectively, by WT or 96KO CD4$^+$ T cells. (C) Lactate secretion to media by WT or 96KO naïve CD4$^+$ T cells cultured for 16 h post CD3/28 activation. Data are mean ± SEM of 3 mice per group, two independent experimental repeats were performed. $^{**}P<0.001$, $^{***}P<0.0001$, 2-tailed Student's *t* test. (D) Extracellular acidification (ECAR) rates in response to glucose, oligomycin, and 2-deoxyglucose additions to 16 hour CD3/28 activated WT or 96KO naïve CD4$^+$ T cells. $^{**}P<0.001$, Area under the curve ANOVA of rates 6–11. Four independent experimental repeats were performed.

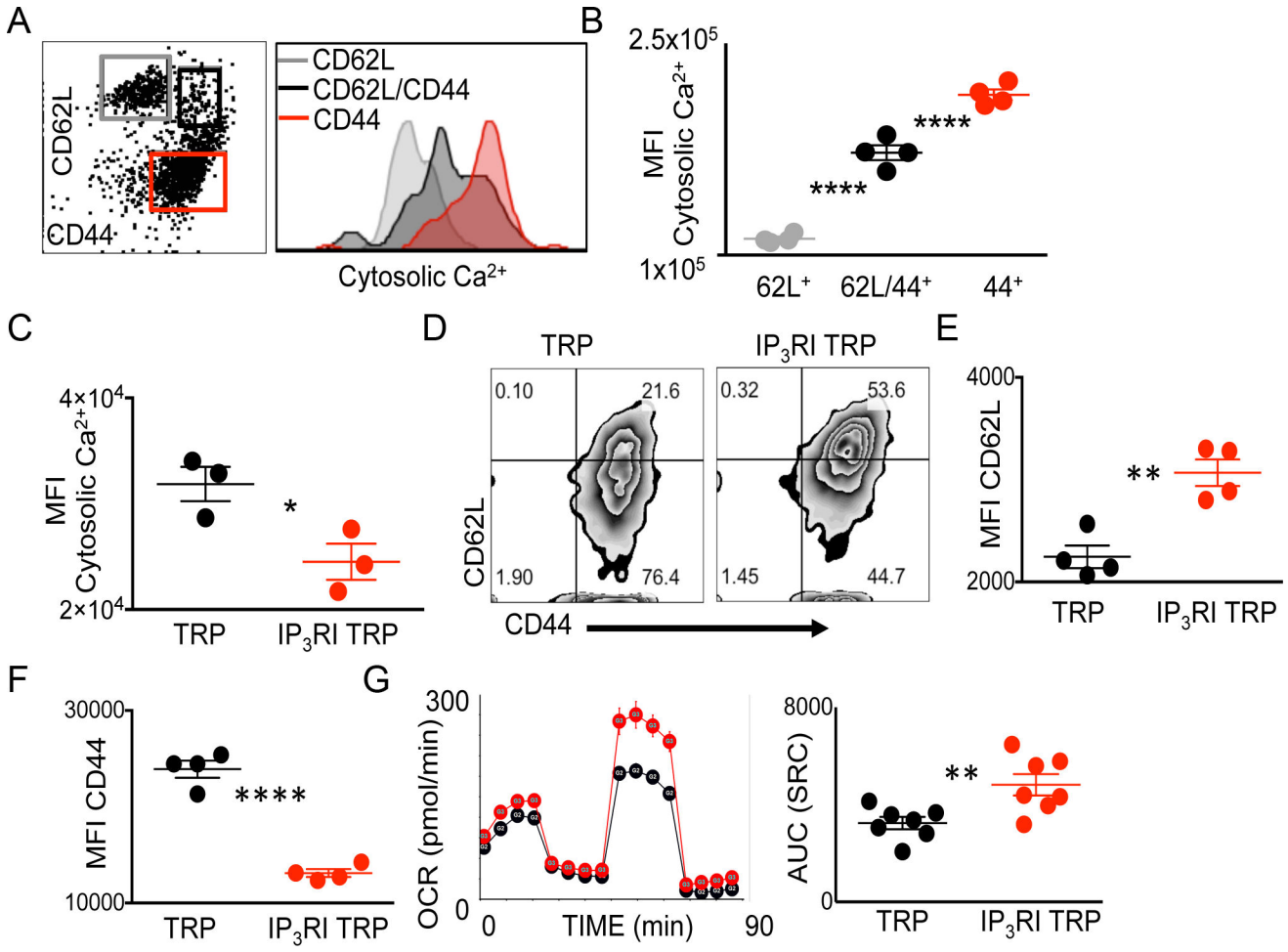

Figure 6. Cell Ca^{2+} differentiates $CD4^+$ T-cell lineages and modulation of IP_3R promotes $CD4^+$ T $CD62L^{high}/CD44^{low}$ phenotype

(A) Representative flow cytometry plots and (B) quantification of WT $CD4^+$ gated splenocytes differentiated by CD62L/CD44 and probed for cytosolic Ca^{2+}. Data are means from 4 mice, three independent experimental repeats were performed. ****$P < 0.0001$, 2-tailed Student *t* test. (C) Quantification of cytosolic Ca^{2+} content in 18 hour *ex vivo* peptide expanded TCR transgenic TRP T cells activated in the presence of IP_3R inhibitor (IP_3RI) 2-APB or vehicle control. (D) Representative flow cytometry plots and quantification of (E) CD62L MFI (F) CD44 MFI of day 7 *ex vivo* expanded TCR transgenic TRP T cells activated in the presence of IP_3RI or vehicle control. (G) Oxygen consumption rates (OCR) and quantification of rates in response to addition of oligomycin, FCCP, and Rotenone/ Antimycin A. (C,E-F) Data are mean ± SEM of individual mice and experiments were repeated at least twice, *$P < 0.05$, **$P < 0.001$,****$P < 0.0001$, 2-tailed Student *t* test. (G) Data are mean ± SEM of pooled T cells from 5–7 mice per group, experiment was repeated 3 times, *$P < 0.05$, Area under the curve ANOVA of rate data, 8–13.

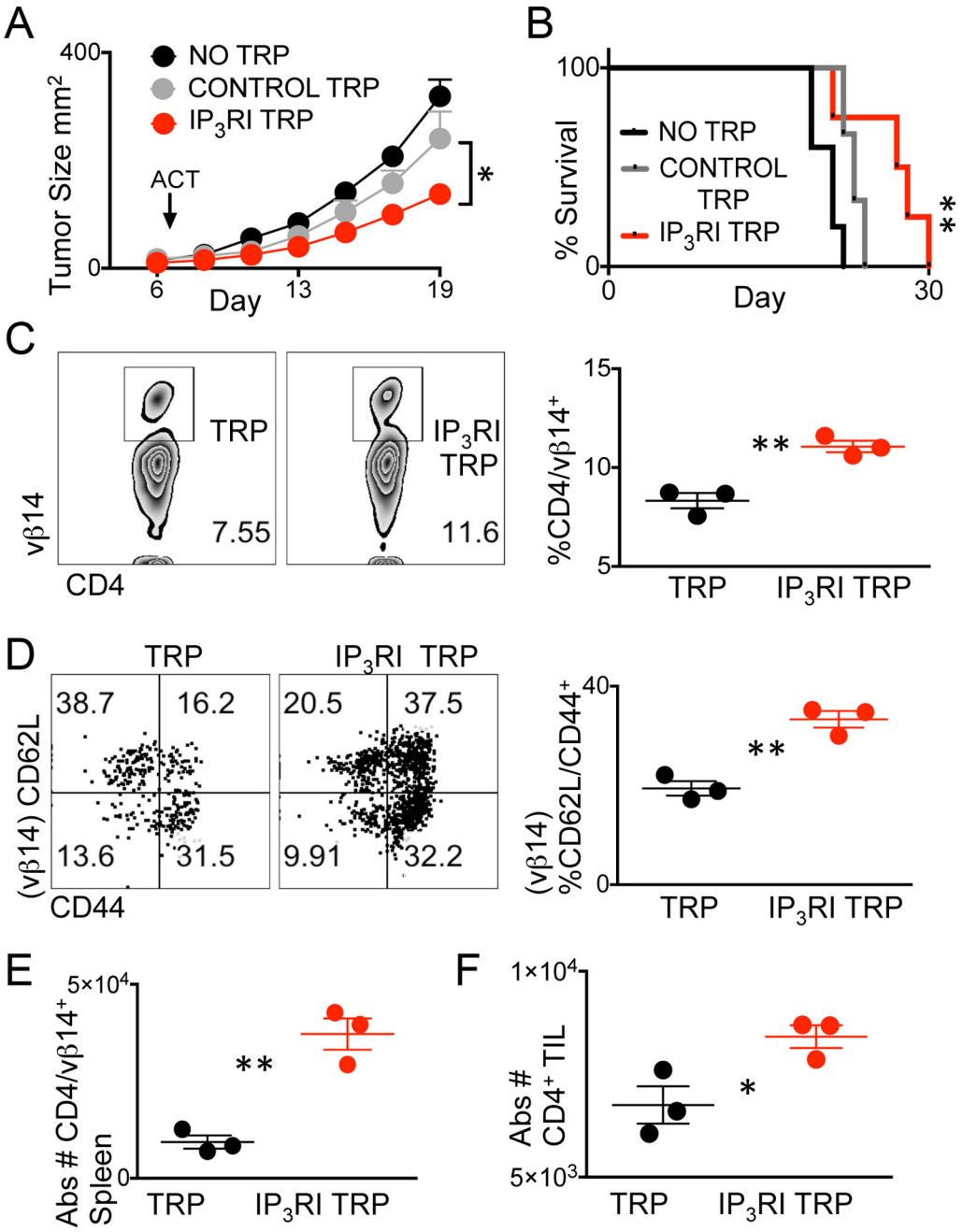

Figure 7. Modulation of cell Ca^{2+} enhances therapeutic efficacy of tumor-specific T Cells

Day 7 established B16F10 tumors were treated with no T cells, or 2 × 10^6 TRP T cells cultured in the presence of IP_3R inhibitor 2-APB (IP_3R TRP) or vehicle control. (A) Tumor growth and (B) survival were measured. Survival endpoints were considered tumor size ≥ 400mm^2 with $n = 5$ mice per group. Experiment was repeated twice. (A) *$P < 0.05$, 2-tailed Student t test of Control TRP versus IP_3RI TRP and (B) **$P < 0.001$, Log-rank test. (C) Representative flow cytometry plots and quantification of CD4/Vβ14$^+$ splenocytes or (D) CD62L/CD44 phenotype of CD4$^+$/Vβ14$^+$ splenocytes,5 days post adoptive cell therapy. (E) Absolute numbers of CD4$^+$/Vβ14$^+$ T cells in spleens or of (F) CD4$^+$ T cell in tumors 5 days

post ACT. (C–F) Data points represent 3 mice per group, *$P < 0.05$, **$P < 0.01$ 2-tailed Student t test.